Desalination and Water Treatment
www.deswater.com

doi:10.5004/dwt.2017.21084

83 (2017) 184–192
July

Theoretical study of various configurations of solar desalination by vacuum membrane distillation

Nader Frikha*, Samira Benabdallah, Slimane Gabsi

Research Unit of Environment, Catalysis and Analysis Process, National Engineering School of Gabes, Rue Omar Ibn El Khattab 6029, Gabes – Tunisia, email: naderfrikha@yahoo.fr (N. Frikha)

Received 24 December 2015; Accepted 24 September 2016

ABSTRACT

Vacuum membrane distillation is a thermal desalination process characterized by a low operating temperature which gives the possibility to coupling with renewable energy. New systems for producing drinking water from seawater using vacuum membrane distillation coupling with solar energy were simulated. The study of different configurations has allowed us to present the processing advantages and disadvantages of each configuration, and enabled us to suggest recommendations on the choice of the configuration according to the type of membrane and application context. In this work, two types of coupling configuration for the type of collectors were investigated. The models concerning the hollow fiber module, the cylindro-parabolic solar collector (CPC) and salinity gradient solar pond (SGSP) were developed. The simulation of the module model allows for the study of the effect of various parameters such us the temperature, velocity and salinity. Then the coupling between this model and the solar collector model was achieved. The solving of models equation allows the determination of each coupling configuration production along the year. The simulation shows that the production of the integrated module in a solar pond is the most productive configuration confirming the interest of the module integration. This system allows the production to reach about 32.5 m^3/y.

Keywords: Solar energy; Desalination; Membrane distillation; Integrated system

1. Introduction

The desalination of seawater might represent the most important source of potable water for arid and semi-arid zones [1]. The technologies of desalination of seawater are operational for many years. But, their cost often limits their utilization to the rich countries. The possibility of designing innovative processes based on the coupling of this technology with solar energy is becoming an attractive way to reduce the production costs and increase the performance of the processes.

Membrane distillation (MD) is a relatively new process that has been investigated worldwide as a conventional separation process [2], such as distillation and reverse osmosis. It is a thermal membrane separation process that involves the transport of vapour through microporous hydrophobic membranes and operates on the principle of vapour–liquid equilibrium as a basis for molecular separation [3–4]. Vacuum membrane distillation (VMD) for seawater desalination is based on the evaporation of solvents through hydrophobic porous membranes improved by applying a vacuum or a low pressure on the permeate side [5]. VMD is the most effective of all DM configurations as it presents the highest flux and desalination rate [6]. Membrane distillation is a process for energy savings compared to other conventional separation processes such as distillation and reverse osmosis [3]. Saffarini et al. have shown that solar heater costs accounted for over 70% of the total cost for all desalination systems, suggesting the desirability of using alternative sources of thermal energy

*Corresponding author.

Presented at the 5th Maghreb Conference on Desalination and Water Treatment — CMTDE 2015, December 21–24, 2015, Hammamet, Tunisia

1944-3994 / 1944-3986

[7]. Given that VMD is characterized by a low operating temperature, the possibility to coupling with renewable energy, such as solar energy has emerged. Various research studies interested in the coupling of solar collectors with VMD were carried out and the possibility of submerging the membrane module in the solar collector was investigated [8–10].

The VMD technique holds important advantages with regard to the implementation of solar driven stand-alone operating desalination systems [11]. Given its geographical location; Tunisia has one of the highest solar fields in the world. The average of solar radiation exceeds 6 kWh/m^3/d for the months May, June, July, August and September [12].

In this work, two types of coupling configuration for each type of collectors were studied. The models pertaining to the module, the CPC and SGSP were developed. The module model simulation allows doing a parametric investigation of the effect of various parameters such us the temperature, velocity and salinity. Then, the coupling between module model and solar collector model was achieved. Their simulation allows the determination of each coupling configuration production along the year.

2. Investigated configurations

The coupling of membrane module with solar energy can be in three possibilities:

- The distillation module is separated from the solar system (system not integrated)
- The module is integrated in the solar collector (integrated system)
- The module is immersed in the solar collector (solar pond)

For the first configuration, the control of the water temperature level feeding the membrane module is possible. In fact, we can provide storage if the temperature admissible by membrane module is exceeded, and we can also use an auxiliary energy when needed.

The second configuration is more original as it makes it possible to reduce the components of the installation and the heating of seawater to be direct. It is necessary to study and evaluate the contribution of the sun and the possibilities of energy storage either in the upstream or in the downstream.

A multitude of separated systems can be conceivable by simply choosing a solar collector to ensure the desired temperature level. A coolant fluid circulates within the solar collector and the heated seawater through a heat exchanger. Several collectors can be proposed, such as flat collector, CPC, PTC, ETV.

Various configurations of membranes modules coupled with the solar collector can be designed. We opted for the study of the coupling of the hollow fiber membrane module with cylindro-parabolic solar collector (CPC) and salinity gradient solar pond (SGSP) (Fig. 1). The hollow fiber module configuration is external-internal. The feed solution flows from outside the hollow fibers and the permeate is collected inside.

For each solar technology, two possibility of coupling were studied:

- Separate and integrated module in an absorber module for CPC.
- Separate and immersed module in the SGSP.

3. Modeling

The developed models take into account the solar flow variation with time as well as the various installation organs operation (membrane module, exchanger ...) [13–15]. A model describing the transfer in the module and the SGSP was developed to study the coupling effect on the module production and compare between the productions of two configurations of the hollow fiber module immerged or not in the SGSP. The different dynamic models were established on the basis of heat and mass balance equations. The scientific interest is that solar flow is variable and intermittent during the day and the whole year. This will lead to a study of the system in transient regime.

3.1. Hallow fiber module

The hollow fiber membrane which can have a large effective area compared with other membrane module types was considered in this work. An external-internal hollow fiber configuration, in which the feed solution flows from outside the hollow fibers and the permeate is collected inside the hollow, was studied.

MD is a thermally driven process based on the principle of vapor/liquid equilibrium and coupled heat and mass transfer [8]. The heat transfer simultaneously occurs with mass transfer whose process influences the rate and coefficients of the heat transfer process, giving birth to a complex heat transfer model [10]. The transfer through the membrane is caused by a partial pressure difference on either side of the membrane. The vapor water molecule was transported through the membrane pores from the higher pressure to lower pressure side. This vapor water molecules transfer through the membrane pores is given by the mechanism of Knudsen diffusion [16–18].

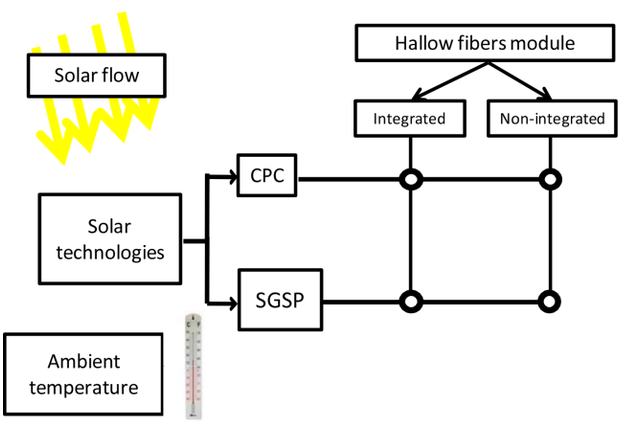

Fig. 1. Investigated configurations.

The water vapor flow density through the internal interface membrane-water (kg·s^{-1}·m^{-2}) is described by the following equation:

$$J_v = K_m \left(P_i - P_{vacuum}\right) \tag{1}$$

The partial pressure P_i was a function of the activity coefficient and the interfacial concentration.

$$P_i = \alpha_{water/NaCl}(1 - X_{NaCl})P_s \tag{2}$$

The water activity coefficient depends on the water concentration in the treated solution [17].

$$\alpha_{water/NaCl} = 1 - 0.5X_{NaCl} - 10X_{NaCl}^2 \tag{3}$$

The interfacial vapor pressure of pure water P_s was evaluated using the Antoine equation as function of interfacial temperature:

$$P_s = \exp\left(23.238 - \frac{3841}{T_i - 45}\right) \tag{4}$$

The coefficient of the membrane permeability or the Knudsen permeability K_m can be related to the membrane structural properties and the membrane interface temperature [16–17].

$$K_m = \frac{2\varepsilon r_p}{3\tau e_m}\frac{1}{RT_i}\sqrt{\frac{8RT_i}{\pi}} \tag{5}$$

So

$$J_V = K_m\left[\alpha_{eau/NaCl}(1 - X_{NaCl})\exp\left(23.238 - \frac{3841}{T_i - 45}\right) - P_{vacuum}\right] \tag{6}$$

The obtained model allows determining the temperature profile inside the module [13–14]. The hollow fibers module characteristics used for this study are shown in Table 1. The module output temperature as well as the flow of distillate are produced as a function of different parameters.

The applied vacuum pressure in this simulation was 4000 Pa and feed velocity was between 0.1 and 1 m/s. The maximum adimissible temperature for this PVDF module was 80°C.

Table 1
Characteristics of hollow fibre module

Nature	PVDF
Internal fibre diameter (mm)	2.6
Membrane thickness (mm)	0.4
Length (m)	1
Fibres number	18
Diameter module (cm)	2
Permeability (m·s^{-1}) (T_i in K)	$K_m = 7.8\ 10^{-6}\ T_i^{0.5}$

3.2. Solar pond (SGSP)

Practically, the solar pond consists of three distinct zones:

- The upper convective zone (UCZ) which is located at the top of the pond. This zone is the absorption and transmission region and contains the low-density salt-water mixture.
- The gradient zone or non-convective zone (NCZ) which contains a variation of salinity increasing with depth. This zone acts as an insulator to prevent heat from escaping to the UCZ, maintaining higher temperatures at lower zones.
- The bottom zone which is the heat storage zone or lower convective zone (LCZ) with uniform salinity.

The energy balance on the volume element of the pond shows that the heat flow accumulated in the volume element is equal to the sum of the inlet flow and absorbed flow minus the out flow. So, the heat transfer process within the solar pond is governed by the following general equation:

$$\frac{\partial(\rho_{sw} Cp_{sw} T_{sw}(t,x))}{\partial t} = \lambda_{sw}\frac{\partial^2 T_{sw}(t,x)}{\partial^2 x} + 0,6\mu_{ex} G_i\, e^{-\mu_{ex}(L-x)} \tag{7}$$

In addition, the mass transfer process within the solar pond is governed by the following general differential equation:

$$\frac{\partial(\rho_{sw} S)}{\partial t} = D\frac{\partial^2(\rho_{sw} S)}{\partial^2 x} \tag{8}$$

With the equation of state of the saline solution given as follows [19]:

$$\rho_{sw} = \rho_{ref}(1 - \alpha_{th}(T - T_{ref}) + \beta_m(S - S_{ref})) \tag{9}$$

Finally, the process of mass and heat transfer in solar pond is described by the system of Eqs. (7) and (8).

We developed a calculation program using the Matlab software computation which solves the differential equation. We used the ode45 function based on the Runge and Kutta method for the resolution that can determine the variations of the different temperatures and the daily distillate flow.

3.3. Cylindro-parabolic collector (CPC)

The absorber is the main component in the CPC, which has the function of absorbing the incident solar radiation, to convert it into heat and transmit it to a heat transfer fluid.

A heat transfer *t* equation between the absorber and the water leads to a partial differential equation of temperature [20]:

$$\rho_w Cp_w \pi\frac{d_{iabs}^2}{4}\Delta z\frac{\partial T_w(t,z)}{\partial t} = -\rho_w Cp_w \dot{V}\frac{\partial T_w(t,z)}{\partial z}\Delta z + q_i(z,t) \tag{10}$$

The q_i is calculated by the equation-Boelter Dittus for fully developed flow in a smoother tube:

$$q_i = h_i\left(T_{abs} - T_w\right)\pi d_{iabs}\Delta z \tag{11}$$

$$\text{with } h_i = 0.023\,\mathrm{Re}^{4/5}\,\mathrm{Pr}^{0.3}\frac{K_w}{d_{iabs}} \tag{12}$$

So, the temperature equation is as follows:

$$\frac{dT_w}{dt} = -\frac{4\dot{V}}{\pi d_{\mathrm{int}\,abs}^2}\frac{dT_F}{dz} + \frac{4h_i}{\rho_w Cp_w d_{iabs}}\left(T_{abs} - T_w\right) \tag{13}$$

The heat balance between the absorber and the environment is described by the following equation:

$$\rho_{abs}Cp_{abs}\frac{\pi}{4}\left(d_{eabs}^2 - d_{iabs}^2\right)\Delta z\frac{\partial T_{abs}\left(t,z\right)}{\partial t} = G_i(t) - q_e(t) - q_i(z,t) \tag{14}$$

with $G_i(t)$ the solar irradiance received by the CPC.

It is assumed that the transfer between the absorber and the environment is only due to convection:

$$q_e(z,t) = h_e\pi d_{eabs}\left(T_{abs} - T_{amb}\right) \tag{15}$$

$$\text{with } h_e = 0.023\,Nu\frac{K_{air}}{d_{eabs}} \tag{16}$$

Thus, the absorber temperature equation is as follows:

$$\frac{\partial T_{abs}}{\partial t} = \frac{G_i(t)w_{abs}}{\rho_{abs}Cp_{abs}\frac{\pi}{4}\left(d_{eabs}^2 - d_{iabs}^2\right)} - \frac{h_e\,\pi\,d_{eabs}}{\rho_{abs}Cp_{abs}\frac{\pi}{4}\left(d_{eabs}^2 - d_{iabs}^2\right)}\left(T_{abs} - T_{amb}\right) - \frac{h_i\,\pi\,d_{iabs}}{\rho_{abs}Cp_{abs}\frac{\pi}{4}\left(d_{eabs}^2 - d_{iabs}^2\right)}\left(T_{abs} - T_w\right) \tag{17}$$

The solar radiation G_i was calculated on the basis of the EUFRAT model and validated by the climatic data of the Sfax region [21].

4. Results and discussion

4.1. Parametric study

4.1.1. Temperature effect

Fig. 2 shows that the outlet temperature increases with the increase in the feed temperature whatever the wall temperature is. This increase becomes smaller by increasing the inlet temperature. For wall temperatures greater than the feed temperature, the outlet temperature remains higher than the feed temperature.

For a wall temperature 120°C and a feed temperature greater than 50°C, the output temperature exceeds 80°C, which is the membrane permissible temperature. But, this temperature is the average of outlet temperature, while the temperature at the membrane interface is always less than the mentioned temperature

The permeate flow increases exponentially with the feed temperature, reaching 20 kg/h·m² for a feed temperature of 65°C and a wall temperature of 120°C. On the other hand, the permeate flux increases with the wall temperature. However, this increase is low for the high feed temperatures, while it is very important for low feed temperatures such as the permeate flow redouble by increasing the wall temperature of 65–120°C although, for feed temperature 70°C, this increase does not exceed 10%.

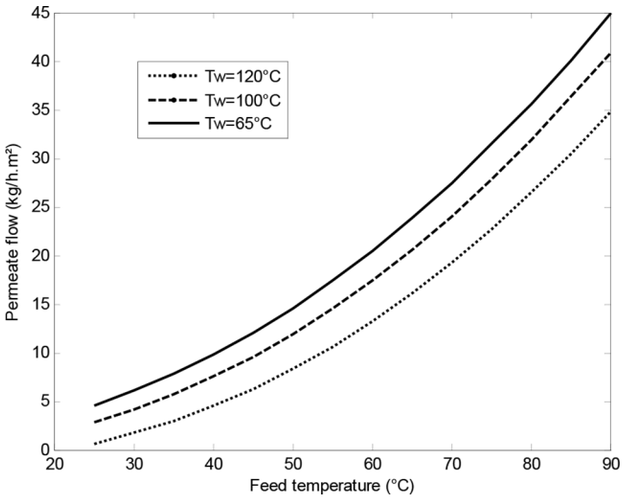

Fig. 2. Permeate flux variation as a function of the feed temperature for three wall temperatures (P_v = 4000 Pa; v_m = 0.5 m/s).

4.1.2. Velocity effect

The permeate flux increases with the wall temperature and velocity. Whatever the velocity value is, for low feed temperatures, the permeate flux is almost nil because the interface membrane temperature does not exceed 30°C (evaporation temperature for a vacuum pressure 4000 Pa) even with high wall temperatures.

By decreasing the velocity, the temperature at the interface increases, and therefore the permeate flow reaches higher values especially at low velocity. It is worthy to note that for a speed 0.1 m/s and a wall temperature at 120°C; the permeate flow is 28 kg/h·m². Thus, according to the study of the feed and wall temperature effect, a low velocity is the best for the increase of the production. But, this condition is limited by the clogging phenomenon and the permissible membrane temperature. Therefore, a moderate velocity is recommended for module operation, which well confirms the velocity choice.

To integrate the module in a solar collector, it was proposed to work with low velocity at start when the solar flow was low, i.e., a low feed and wall temperatures.

4.1.3. Salinity effect

Fig. 4 shows that the permeate flow decreases as the feed concentration increases. Actually, the decrease is very remarkable for high feed temperatures, while it is almost constant for low feed temperatures. This is generally due to

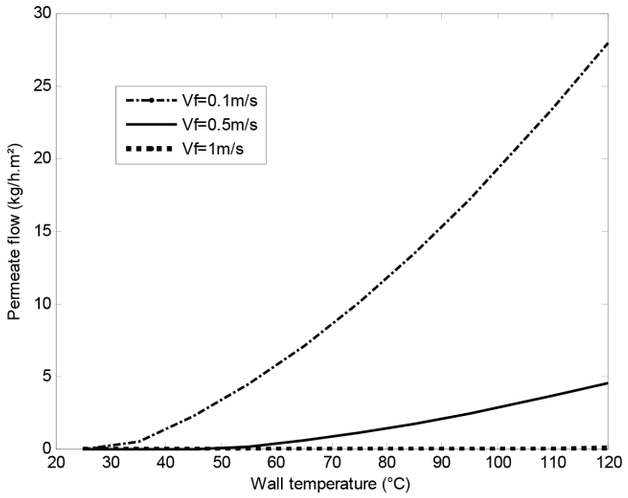

Fig. 3. Permeate flow variation with the wall temperature at different velocities (P_v = 4000 Pa; T_{feed} = 25°C).

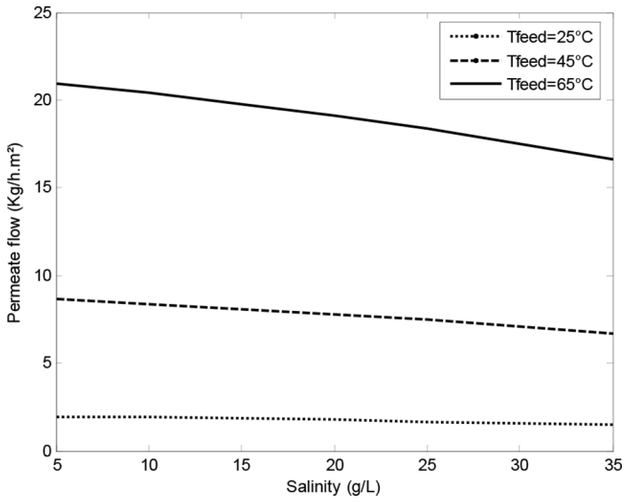

Fig. 4. Permeate flow variation of salt concentration for three different feed temperatures (P_v = 4000 Pa; v_m = 0.5 m/s).

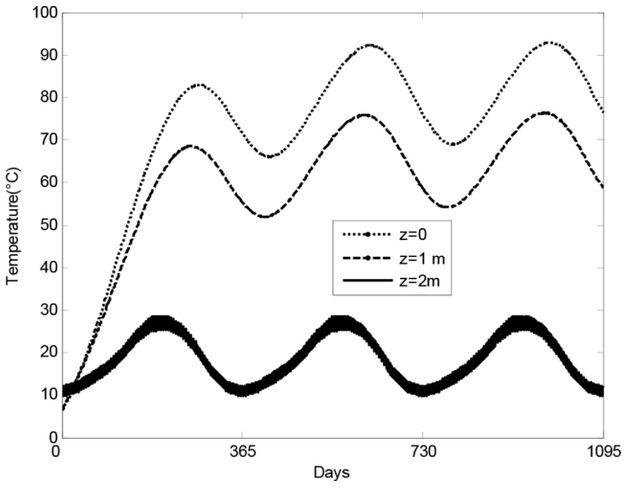

Fig. 5. Instantaneous temperature variation for three years.

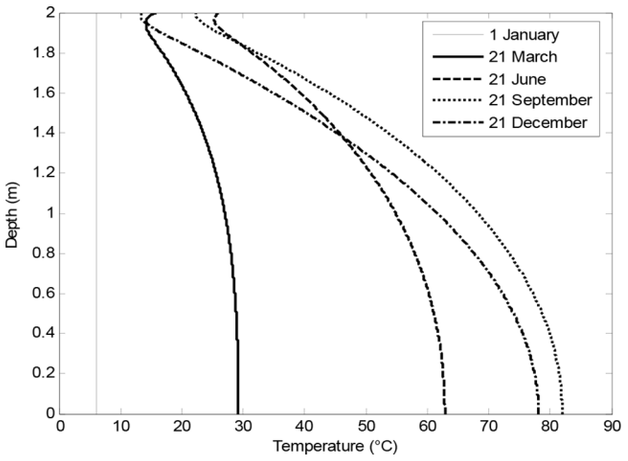

Fig. 6. Temperature variation according to the depth for 4 typical days.

the reduction of the water vapor pressure as a result of the reduction of the water activity coefficient.

4.2. SGSP

The SGSP operation started on 1 January. For a fixed date, the temperature was calculated using the energy accumulated in the SGSP from the start date. For this reason, the temperature at the end of the year was greater than that of the beginning. Fig. 5 shows that the upper zone temperature is near ambient temperature, since the losses are higher in this zone. The temperature of the salt water reaches its maximum during the summer when the solar radiation is maximal. The highest temperature is the pond bottom; it is in the order of 83°C.

Fig. 6 represents the temperature according to the depth for four typical days. It should be noted that these profiles were taken at a specific time, precisely at 12:00 of each day.

The temperature in the SGSP, for January 1, is the ambient temperature. Fig. 6 shows that, while approaching the SGSP bottom, the salt water temperature increases with the increase in salinity. Therefore, the largest quantity of energy is absorbed by the concentrated salt solution at the bottom of the SGSP. Similarly, for the bottom, the temperature variation varies slowly until the temperature becomes almost constant, thereby forming the LCZ zone. On the other hand, the temperature varies differently for four typical days, in which it varies slowly to the cold months (September and December), while the variation is important for hot months (March and June). The solar heating effect within the pond is more important than for the cold season. Besides, for the cold season, in particular for the winter, heat losses towards the ambient are more important due to colder air temperature.

For the top portion (UCZ) where the temperature is close to the ambient temperature, the cooling effect of water can be clearly observed, in addition to the effect of the energy accumulated within the pond where these low deviation for March and June. This deviation disappeared for September and December thereby forming the UCZ zone.

For the intermediate portion (NCZ), where salinity increases with depth, it behaves as transparent heat insulation. In fact, it is crossed by the solar radiation which is absorbed and trapped by the very salty water at the bottom. For this zone, the temperature profiles remain essentially linear, then it is slowly varied and the solar heating effect depends on the month. Despite the low ambient temperature and solar radiation for September and December the temperature is higher than in June reaching 82°C. The solar heating effect due to the heat loss (low ambient temperature and solar radiation) is about 5°C from September to December.

Two configurations were studied; the first of which was a module membrane in series with SGSP (Fig. 7a), and the second one was a hollow fiber module immerged in the SGSP (Fig. 7b).

The SGSP depth was 2 m.We has established calculation models to simulate the desalination system operation. From these models, we developed calculation programs on the software MATLAB in order to simulate the functioning of different configurations.

To compare the two configurations of the fiber module we calculated the daily distillate quantity produced for the same operating conditions. Fig. 8 represents the daily production variation along three years. Module production began only at 80 d when the desired temperature level was reached. Fig. 8 shows that the daily production of the immersed module is greater than that of the separated module. The immersed module production presents more than one and a half times that of the separated module, exceeding the 75 kg/d per m² of membrane. The third yearly immersed module production is 16.8 m³, which represents more than one and half times the separated module production. Thus, immersing the module in the solar pond was found to improve the performance of the hollow fiber module.

4.3. CPC

In the present work, the surface of the adopted CPC was 18 m², the feed temperature was equal to the ambient temperature and the feed flow was 257 kg/h. The obtained model allows the determination of the absorber temperature (Fig. 9) and the CPC outlet temperature (Fig. 10) along the day for the four typical days.

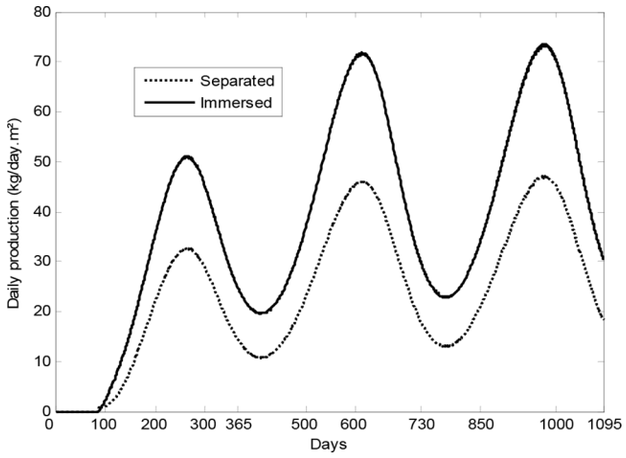

Fig. 8. Daily production variation along three years.

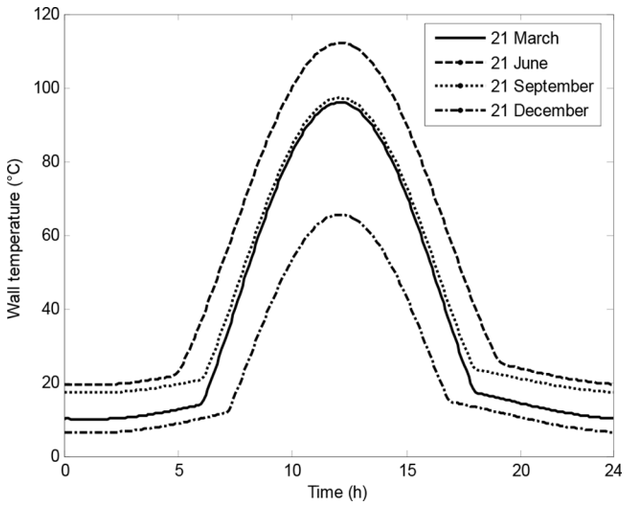

Fig. 9. Instantaneous variation of wall temperature for 4 typical days.

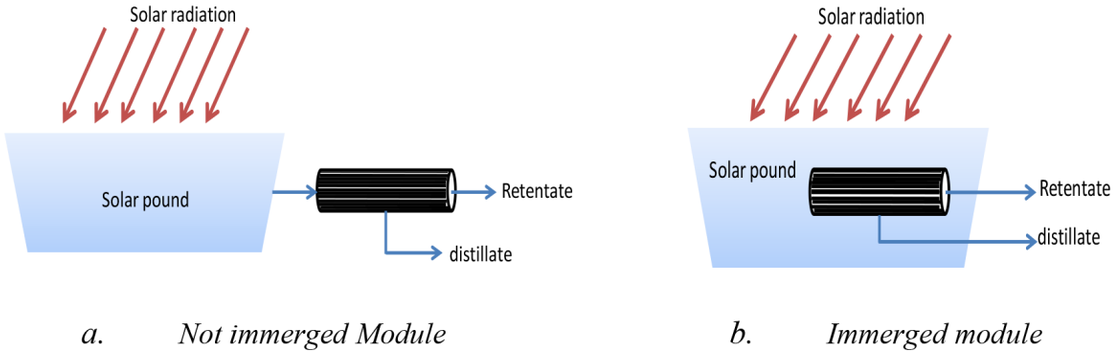

a. Not immerged Module *b. Immerged module*

Fig. 7. Coupling VMD with a SGSP.

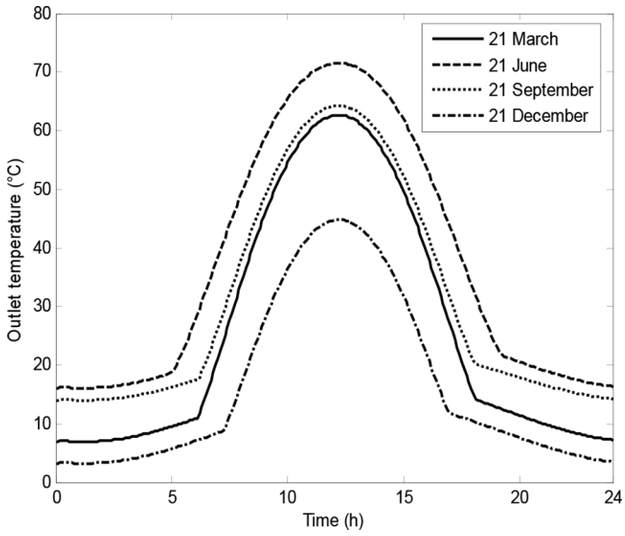

Fig. 10. Instantaneous variation of CPC outlet temperature for 4 typical days.

The absorber temperature variation followed the same shape as the solar flow, and reached a maximuum of 115°C at noon for the month of June and 65°C for the month of December. Based on this temperature and the CPC feed temperature (ambient temperature), the instantaneous variation of the temperature at the CPC outlet along the day (Fig. 10) is obtained.

Moreover, the outlet CPC temperature variation was found to follow the same pace as the inlet temperature, reaching a maximuum of 68°C at noon for the month of June. So, it is always lower than the permissible temperature by the membrane (80°C).

To compare the two configurations of the fiber module (integrated or non-integrated), we determine the permeate flow instantaneous variation for the same operating conditions.

It is worthwhile to note that for the case of the hollow fiber module integrated in the CPC, the surface of the membrane depends on the collecting area because the membrane module is integrated in the absorber.

Fig. 13 shows that the permeate flow reached a maximum at the hours when the received sunshine by the collector was higher. This maximum reached 6.8 $kg{\cdot}h^{-1}{\cdot}m^{-2}$ of the membrane for the integrated module and 4.8 $kg{\cdot}h^{-1}{\cdot}m^{-2}$ for the separated module. The permeate flow for the integrated configuration is always higher than that of the non-integrated one. The effect of the integration of the hollow fiber module in the CPC on the production of the module exceeded the 30% of the flow produced by the non-integrated fiber module.

The integration of the hollow fiber module in the solar collector was proven to improve the desalination unit performance.

4.4. Comparison

To compare the two configurations (separated and integrated) of the hollow fiber module, we calculated the daily

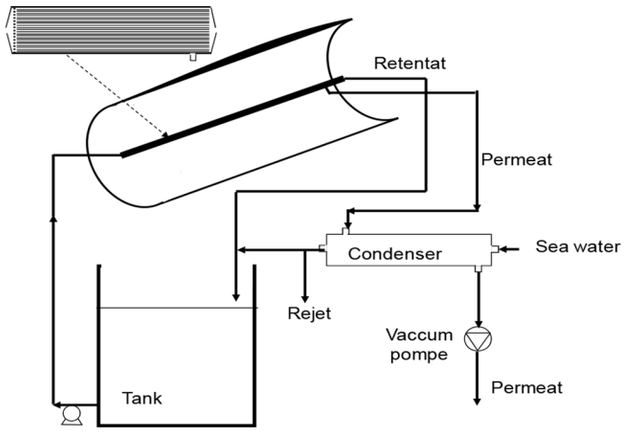

Fig.11. Hollow fiber module integrated within CPC.

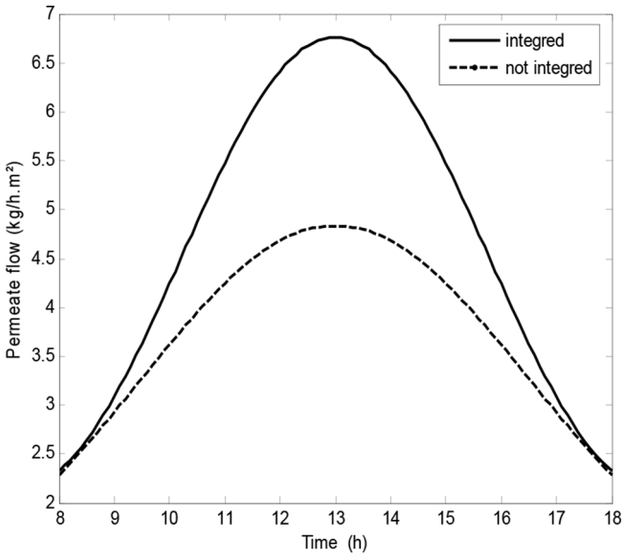

Fig. 12. Instantaneous variation of the permeate flow for the two configurations. S_{CPC} = 18 m^2, 21 June.

distillate quantity produced for the same operating conditions. The results obtained are illustrated in Table 2.

Table 1 shows that the daily production of the module immerged in the SFGP is greater than the production obtained with other configurations. It should be noted that the most limiting agent for this configuration is the high salinity. Indeed, for this operating mode, the fibers come in contact with highly saline water, which will cause problems of polarization and fouling. In the case of coupling with the CPC, integrated module production exceeded 30% of that of the non-integrated module.

Although the integration of the module in a solar collector improves desalination unit performance, we can achieve higher productivity in the separate systems case because a sufficient collecting surface can be placed to ensure the desired production. This is not the case for the integrated configurations. In fact, it is thermally limited because of the geometric dependence between the collecting area and

Table 2
Comparison of annual production (m^3/m^2) between two modules configurations

	Not integrated	Integrated
Solar pound	13.7	32.5
CPC	11.4	18.2

membrane surface. Thus it will be thermally limited and membrane operating below its nominal capacity.

The comparative study has shown that in both studied cases, the integration of membrane module improves productivity. Indeed, given the fact that seawater must necessarily circulate in the solar collector, it is necessary to use noble materials for the construction of the collector (e.g. titanium). This problem does not arise in the case of the configuration where the membrane module is separated from the collector. Actually, the coolant fluid circulates within the collector, the fluid transfers the sun calories won from the sun to water via a heat exchanger. Under these conditions, only the exchanger is built in noble materials. On the one hand, these materials have generally a less conductivity and, on the other, their price is exhaustive. A second constraint is the large gap between the required membrane surface and the necessary collector surface, because for 1 m^2 membrane area, 10 m^2 collector surface are necessary for the functioning of the membrane. This problem can be solved with concentrating collectors.

One of the problems with concentration collectors (CPC, PTC...) that only the external/internal configuration is possible, view that seawater must circulate outside the fibers to be in contact with the absorber and to be able to overheat. Knowing that most commercial modules are internal/external configuration, the issue of acquisition modules external/internal configuration should be taken into account.

On the other hand, the improvement of productivity is mainly observed in the case where the velocity is low (below 0.4 m/s). This velocity must be very low to increase the passage time of water in the absorber and thus to achieve acceptable temperature levels. These velocities are not adequate for the functioning of membranes. In fact, the velocity needs to be greater than 0.5 m/s in order to minimize the fouling of the membrane.

For coupling with SGSP, the module production is limited by salinity bearing in mind that the salinity is very high in the zones of the desired level of temperature. Considering the idea of agitation to reduce salinity to have less fouling, it was found to be undesirable in the case of SGSP as it will disrupt the stability of the pond.

5. Conclusions

The study of different configurations has proven the benefits of integrating membrane module in the solar collector. This possibility reduces heat loss and has a compact installation, which leads to improved productivity. However, the integration is facing several technical limitations. This separation has the advantage of not being energetically limited because the choice of the collector surface is geometrically independent of the membrane surface. In addition, it reduces the cost of the installation because we would not be obliged to use materials resistant to corrosion.

Symbols

D_i	—	Diffuse radiation on a flat surface
D	—	Coefficient of salt diffusion
G_i	—	Solar radiation
P_s	—	Vapor pressure
P_{vacuum}	—	Vacuum pressure
S	—	Salinity
Q_m	—	Mass flow
Q	—	Heat flow
R	—	The ideal gas constant
T	—	Temperature
X_{NaCl}	—	Salt molar fraction

Greek

$\alpha_{eau/NaCl}$	—	Water activity coefficient
ε	—	Membrane porosity
Φ	—	Inclination angle
λ	—	Heat conductivity
μ	—	Dynamic viscosity
μ_{ex}	—	Extension coefficient
θ_{inci}	—	Angle of incidence
ρ	—	The salt water density
τ	—	Membrane tortuosity

Indices

amb	—	Ambient
abs	—	Absorbed
f	—	Feed
o	—	Out
sw	—	Sea water

References

[1] V. Calabrol, E. Drioli, Polarization phenomena in integrated reverse osmosis and membrane distillation for seawater desalination and waste water treatment, Desalination, 108 (1996) 81–82.

[2] Z. Ding, R. Ma, A.G. Fane, A new model for mass transfer in direct contact membrane distillation, Desalination, 15l (2002) 217–227.

[3] S. Al-Obaidani, E. Curcio, F. Macedonio, G. Di Profio, H. Al-Hinai, E. Drioli, Potential of membrane distillation in seawater desalination: Thermal efficiency, sensitivity study and cost estimation, J. Membr. Sci., 323 (2008) 85–98.

[4] A. Kargari, M. Mahdi, A. Shirazi, Water Desalination, Solar-Assisted Membrane Distillation, Encyclopedia of Energy Engineering and Technology, 2nd ed., 2015; pp. 2095–2109.

[5] J. Phattaranawik, R. Jiraratananon, A.G. Fane, Heat transport and membrane distillation coefficients in direct contact membrane distillation, J. Membr. Sci., 212 (2003) 177–193.

[6] Ch. Huayan, W. Chunrui, J. Yue, W. Xuan, L. Xiaolong, Comparison of three membrane distillation configurations and seawater desalination by vacuum membrane distillation, Desal. Water Treat., 28 (2011) 321–327.

[7] J.-B. Gálveza, L. García-Rodríguezb, I. Martín-Mateosclination, Seawater desalination by an innovative solar-powered membrane distillation system: the MEDESOL project, Desalination, 246 (2009) 567–576.

[8] Wang, L. Zhang, H. Yang, H. Chen, Feasibility research of potable water production via solar-heated hollow fiber membrane distillation system, Desalination, 247 (2009) 403–411.
[9] J. Mericq, S. Laborie, C. Cabassud, Evaluation of systems coupling vacuum membrane distillation and solar energy for sea water desalination, Chemical Eng. J., 166 (2011) 596–606.
[10] Zhang, Y. Peng, S. Ji, Z. Li, P. Chen, Review of thermal efficiency and heat recycling in membrane distillation processes, Desalination, 367 (2015) 223–239.
[11] E. Saffarinia, K. Summersb, H.A. Arafata, Economic evaluation of stand-alone solar powered membrane distillation systems, Desalination, 299 (2012) 55–62.
[12] S. Bouguecha, B. Hamrouni, M. Dhahbi, Small scale desalination pilots powered by renewable energy sources: case studies, Desalination, 183 (2005) 151–165.
[13] S. Ben Abdallah, N. Frikha, S. Gabsi, Simulation of solar vacuum membrane distillation unit, Desalination, 324 (2013) 87–92.
[14] S. Ben Abdallah, N. Frikha, S. Gabsi, Study of the performances of different configurations of seawater desalination with a solar membrane distillation, Desal. Water Treat., 52(13–15) (2014) 2362–2371.
[15] N. Frikha, R. Matlaya, R. Chaouachi, S. Gabsi, Simulation of an autonomous solar vacuum membrane distillation for seawater desalination, Desal. Water Treat., 52(7–9) (2014) 1725–1734.
[16] Abu-Zeid, Y. Zhang , H. Dong, L. Zhang , H.-L. Chen, L. Hou, A comprehensive review of vacuum membrane distillation technique, Desalination, 356 (2015) 1–14.
[17] D. Lawson, R. Lloyd, Membrane distillation, J. Membr. Sci., 124 (1997) 1–25.
[18] Dao, J.P. Mericq, S. Laborie, C. Cabassud, A new method for permeability measurement of hydrophobic membranes in vacuum membrane distillation process, Water Res., 47 (2013) 2096–2104.
[19] R.B. Mansour, C.T. Nguyen, N. Galanis, Transient heat and mass transfer and long-term stability of a salt-gradient solar pond, Mech. Res. Commun., 33 (2006) 233–249.
[20] W. Chekirou, N. Boukheit, T. Kerbache, Various modes of heat transfer in an absorber of a cylindrical parabolic solar concentrator, ICRESD-07, Tlemcen, 2007, pp. 21–28.
[21] S. Ben Abdallah, étude d'une unité de dessalement solaire membranaire sous vide: modélisation, simulation et optimisation des conditions opératoires. Theses ENIG, Tunisia, 2015.